Applied Physics Letters ARTICLE pubs.aip.org/aip/apl

Enhanced resistive switching characteristics of conductive bridging memory device by a Co–Cu alloy electrode

Cite as: Appl. Phys. Lett. **123**, 133504 (2023); doi: 10.1063/5.0160380
Submitted: 1 June 2023 · Accepted: 8 September 2023 ·
Published Online: 26 September 2023

Calvin Xiu Xian Lee,[1,2] Putu Andhita Dananjaya,[1] Mun Yin Chee,[1] Han Yin Poh,[1,2] Funan Tan,[1] Jia Rui Thong,[1,2] Lingli Liu,[1] Gerard Joseph Lim,[1] Yuanmin Du,[1] Juan Boon Tan,[2] and Wen Siang Lew[1,a)]

AFFILIATIONS

[1]School of Physical and Mathematical Sciences, Nanyang Technological University, 21 Nanyang Link, Singapore 637371
[2]GlobalFoundries, 60 Woodlands Industrial Park D Street 2, Singapore 738406

[a)]Author to whom correspondence should be addressed: wensiang@ntu.edu.sg

ABSTRACT

One of the main challenges in the development of conductive bridging random access memory (CBRAM) is the large stochastic nature of ion movement that ultimately leads to large parameter variability. In this study, the resistive switching variability of CBRAM devices is significantly improved by employing Co–Cu alloy as the active electrode. By comparing with Pt/Ta_2O_5/Co devices, the $Co_{70}Cu_{30}$ alloy exhibited lower forming voltage (<2 V), lower SET voltage (<0.70 V), and faster response time (~70 ns). The filament stability indicated by the distribution of SET/RESET voltage and high resistance state/low resistance state variation was significantly improved. Our experimental results suggest the formation of Co filaments, and the proposed mechanism is governed by the galvanic effect. In addition, a comparison between $Co_{70}Cu_{30}$ and $Co_{30}Cu_{70}$ alloys highlights that the relative proportion between Co and Cu plays an essential role in the device performance. A physical model based on different electrochemical activities of the alloys has been proposed to explain the filament formation and the improved switching uniformity in the $Co_{70}Cu_{30}$ alloy. This study not only develops a CBRAM with enhanced performance but also advances the implementation of suitable alloy systems for the application of such devices.

With a simple metal–insulator–metal (MIM) structure, resistive random access memory (ReRAM) has attracted great attention in recent years, with the strong technological demand to develop next-generation memory devices,[1–4] reconfigurable logic circuits,[5,6] and neuromorphic computing applications.[7–9] Among the various types of resistive switching devices, a typical conductive bridge random access memory (CBRAM) consists of an electrochemically active electrode (AE) and an inert electrode (IE), separated by a thin solid electrolyte layer.[10,11] The reversible resistive switching mechanism of CBRAM is based on electrochemical metallization (ECM), which involves the nucleation and migration of metal ions (e.g., Ag[12,13] or Cu[14–16]) through the solid electrolyte under an external electric field to form conductive filaments.[17,18] Due to its high *k*-dielectric constant and compatibility with the complementary metal oxide semiconductor (CMOS) fabrication process, Ta_2O_5 is considered as one of the most promising solid electrolytes for CBRAM.[19–21] Among the various pure metal-based electrochemically active electrodes, Cu is a preferred material due to its abundance, low cost, and relatively low solubility with the electrolyte layer.[22–24] More recently, Co-based CBRAMs have been reported, with the advantages in low operating current, excellent retention, and CMOS-compatible fabrication capability.[25–27] Nonetheless, the pure metal-based CBRAM still exhibits large switching variability and performance degradation due to its large stochasticity of the ion movement, which inhibits further technological development of this memory technology.[23,28,29] The stochastic nature of the conductive filament formation and dissolution in CBRAM plays a significant role in the device performance.[30,31] In comparison, electrode alloying provides a new degree of freedom for controlling electrochemical activity, nucleation sites, ion migration, and filament formation.[32–35] By employing an Au–Ag alloy electrode, the forming voltage, resistive switching stability, and speed were reported to be significantly enhanced due to the galvanic effect between Au and Ag.[33–35] Using the Ag–Cu alloy electrode, the switching performance was also improved through the formation of Cu filaments, with the composition identified by transmission electron microscopy (TEM).[36,37] However, there has not yet been an investigation of how the Co–Cu alloy influences the resistive switching properties of CBRAM.

In this work, we investigated the resistive switching behavior of the MIM device structures consisting of Pt/Ta_2O_5/AE, where AE is varied with different active electrode materials, namely, Co, Cu, $Co_{70}Cu_{30}$, and $Co_{30}Cu_{70}$. The $Co_{70}Cu_{30}$ alloy electrode CBRAM exhibits reduced electroforming voltage along with smaller SET/RESET voltages variation, improved resistance states uniformity, and faster response time. The morphological analysis of the Co–Cu alloy surface revealed that the resistive switching improvement can be attributed to the preferential oxidation of Co within the Co–Cu alloy system, also known as the galvanic effect. A physical model based on the galvanic effect is proposed to explain the origin of the different resistive switching performances.

The fabrication of the devices begins with inert electrode patterning onto a SiO_2 substrate via UV lithography. Following a Ti (2 nm) adhesion layer deposition, Pt (10 nm) inert electrode was deposited via direct current (DC) magnetron sputtering with 20 sccm Ar gas flow rate at a working pressure of 2 mTorr and sputtering power 50 W. The patterned Pt inert electrode is formed via a liftoff process. Subsequently, the active electrode patterning was performed, followed by a Ta_2O_5 (7 nm) electrolyte layer and Co–Cu alloy (50 nm) active electrode deposition. The electrolyte layer is deposited via radio frequency (RF) magnetron sputtering with 20 sccm Ar gas flow rate at a working pressure of 2 mTorr, utilizing a 2 in. ceramic target of Ta_2O_5, while the Co–Cu alloys are deposited via DC magnetron sputtering with 20 sccm Ar gas flow rate at a working pressure of 2 mTorr. The composition of the Co–Cu alloys was obtained by co-sputtering the 2 in. Co and Cu targets at varying power levels ($Co_{70}Cu_{30}$/144 W: 28 W and $Co_{30}Cu_{70}$/61 W: 67 W) with a fixed deposition time of 400 s to achieve the desired deposition rates. A Pt capping layer (5 nm) was deposited to protect the device. The chamber atmosphere during all the sputtering processes of all the films consisted of 2 mTorr Ar gas and the target-to-substrate distance was consistently maintained at 200 mm. The fabrication process is finalized by performing a liftoff process to obtain the Pt/Ta_2O_5/Co–Cu alloy/Pt CBRAM structure, as illustrated in Fig. 1(a).

Figure 1(b) shows the optical image of the fabricated CBRAM device, where a 10×10 μm^2 cell size of the experimental devices is formed. X-ray photoelectron spectroscopy (XPS) characterization determined the nominal mole or atomic fraction (at. %) of the Co–Cu alloy electrodes as Co: Cu = 70%: 30% for the Co-rich alloy, and Co: Cu = 30%: 70% for the Cu-rich alloy. The XPS spectra are presented in the supplementary material as Fig. S1, where Kratos Axis Supra XPS system was used for analysis. To perform the electrical characterization of the Pt/Ta_2O_5/Co–Cu alloy CBRAM devices, a Keithley 4200A semiconductor parameter analyzer was utilized by grounding the inert electrode and biasing the active electrode. In addition, Pt/Ta_2O_5/Ag–Cu alloy CBRAMs are also fabricated as a reference.

Figures 1(c)–1(f) show DC–voltage (I–V) curves of the CBRAM devices, with the compliance current (I_{CC}) set at 1 mA. The resolution of the voltage sweeping is 5 mV per step. All the CBRAM devices in the pristine state show an initial resistance value of $\sim 10^8$ Ω with a 0.2 V read voltage, indicating a good consistency between the Ta_2O_5 films. An electroforming process (0 V → +3 V) is required before the device can be reversibly switched between a high resistance state (HRS) and a low resistance state (LRS). A bipolar switching characteristic has been observed for all the devices. When a positive set voltage (V_{SET}) is applied, the device switches from HRS to LRS, and when a negative reset voltage (V_{RESET}) is applied, the device switches from LRS to HRS. Among the pure metal-based CBRAM devices, a higher electroforming voltage ($V_{Forming}$) is observed for the Co-based device [Fig. 1(c)], compared to that of the Cu-based device [Fig. 1(d)]. This can be ascribed to the different diffusion capability of Cu and Co ions into the Ta_2O_5 insulator matrix, to form conductive bridges between the active and inert electrodes. For the following resistive switching operations (100 switching cycles), although relative smaller V_{SET} and V_{RESET} values have been observed for the Cu-based device [Fig. 1(d)], a wider switching distribution is observed, which indicates a great disadvantage in contrast to that of the Co-based device [Fig. 1(c)]. The distribution of V_{SET}, V_{RESET}, and $V_{Forming}$ for different devices is shown in Fig. S2.

By comparing with the pure metal-based devices, an enhancement of the device performance has been observed, when a $Co_{70}Cu_{30}$ alloy is selected as the active electrode material. Figure 1(e) shows I–V curves of a Pt/Ta_2O_5/$Co_{70}Cu_{30}$ device, with $V_{Forming}$ at ∼2 V, which is significantly reduced compared to that of a Co-based device with $V_{Forming}$ at ∼2.6 V [Fig. 1(c)]. More interestingly, an even more stable switching characteristic is shown for the $Co_{70}Cu_{30}$ alloy-based device, with V_{SET} and V_{RESET} varying in a much smaller range. For comparison on the resistive switching performance of the Co–Cu alloy, another device with $Co_{30}Cu_{70}$ as the AE has also been fabricated, with the I–V curves shown in Fig. 1(f). A decreasing of the Co percentage results in a further reduction of the $V_{Forming}$ [Fig. S2(d)]. However, a degradation of the device performance is observed where both V_{SET} and V_{RESET} shift into a wider range from cycle to cycle, and an unstable switching characteristic is presented.

Figures 2(a) and 2(b) show the cumulative probability distribution of the V_{SET}/V_{RESET} and the resistance states during 100 continuous DC switching cycles for the CBRAM devices shown in Figs. 1(c)–1(f). A boxplot of the resistance of the HRS and LRS of each CBRAM device is shown in Fig. S3. For the $Co_{70}Cu_{30}$ alloy-based device, both V_{SET} and V_{RESET} and the resistance states (HRS and LRS) show narrow distributions, indicating significant enhancements of the resistive switching. The V_{RESET} and V_{SET} ranges are −0.94 to −0.51 V and 0.44 to 0.88 V, respectively, which are much narrower than those of the other devices. The average/standard deviation (SD) of the operating voltages is −0.65 V/0.07 V (V_{RESET}) and 0.68 V/0.07 V (V_{SET}). With the Cu-based device as an example, V_{RESET} ranges from −0.99 to −0.18 V (SD, 0.19 V), and V_{SET} ranges from 0.18 to 1.22 V (SD, 0.23 V). The SD of the V_{RESET} and V_{SET} is reduced by 69.9% and 63.2%, respectively, for the $Co_{70}Cu_{30}$ alloy-based device, in comparison with that of Cu. Similarly, for the HRS/LRS distribution [Fig. 2(b)], a much narrower distribution is also observed for the $Co_{70}Cu_{30}$ alloy-based device. Although the other CBRAM devices typically show a larger memory window (or resistance switching ratio), the large variation of the resistance values (HRS) had a great disadvantage of these devices for memory storage applications. Among the alloy electrode CBRAMs, the resistive switching properties of Ag–Cu alloy-based CBRAM have been extensively investigated, making it suitable as a reference stack for comparison.[7,36–38] Between the fabricated Ag–Cu alloy-based CBRAM and Co–Cu alloy-based CBRAM, the $Co_{70}Cu_{30}$ alloy also shows the advantage on the uniformity of switching operations (see Figs. S4 and S5 for more details). Qiao *et al.*[36] reported that Cu filaments are formed in the Ag–Cu alloy-based CBRAMs, which is attributed to the galvanic effect. The nature of the conductive filaments

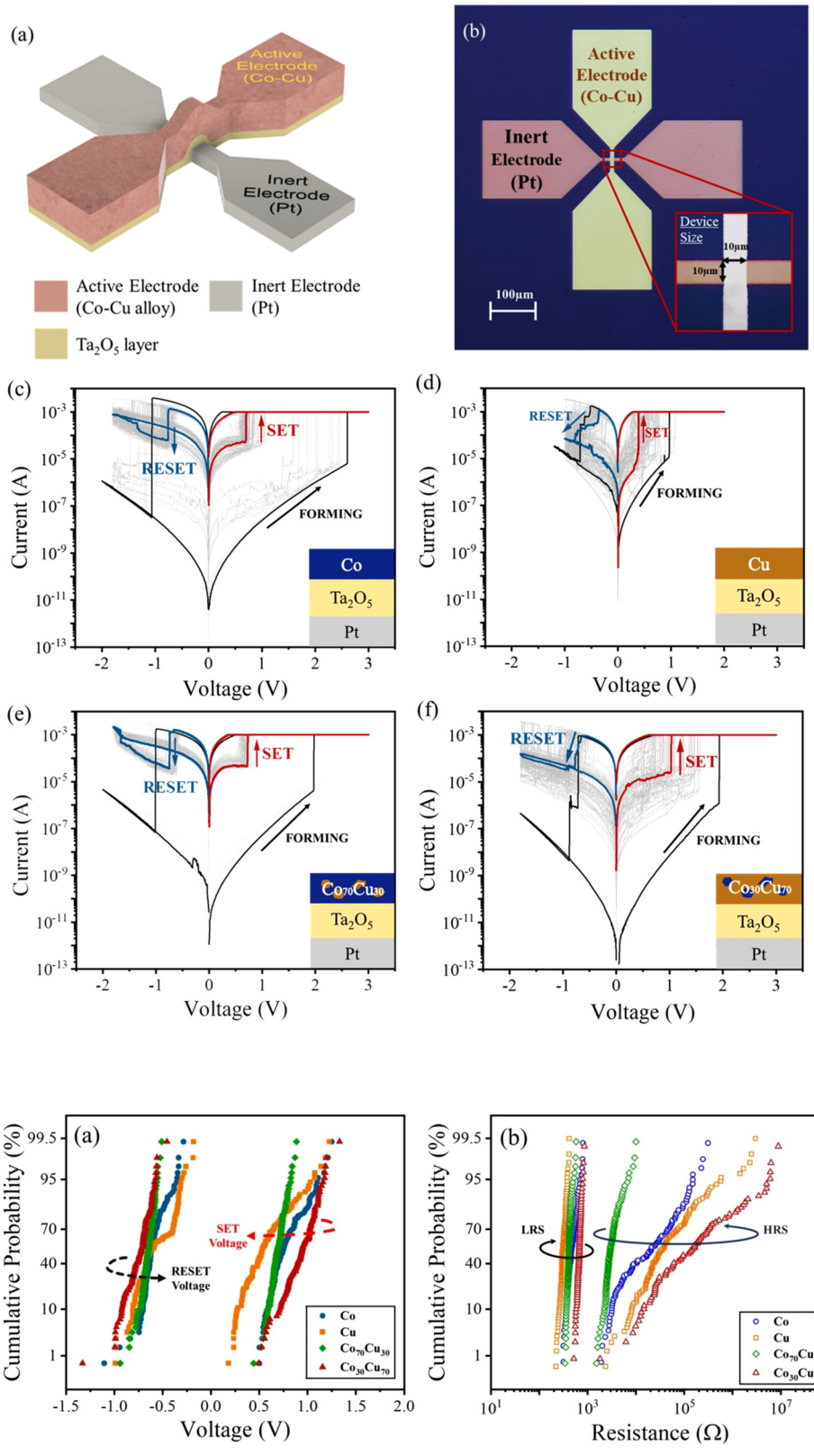

FIG. 1. (a) Schematic illustration of the CBRAM device structure where the electrolyte layer (Ta_2O_5) is sandwiched between the active electrode (AE) and inert electrode (IE). (b) Optical image of a fabricated Co–Cu alloy-based CBRAM device. I–V measurements of CBRAM devices with different active electrode: (c) Pt/Ta_2O_5/Co, (d) Pt/Ta_2O_5/Cu, (e) Pt/Ta_2O_5/$Co_{70}Cu_{30}$, and (f) Pt/Ta_2O_5/$Co_{30}Cu_{70}$. The plots represent 101 cycles of sweeping loops, with the red and blue curves representing the typical SET and RESET operations, and the black curve representing the initial forming and the first RESET after the forming operations, respectively.

FIG. 2. Cumulative probability of (a) V_{SET} and V_{RESET} and (b) HRS/LRS over 100 continuous DC sweeping cycles for CBRAM devices with different active electrodes, Co, Cu, $Co_{70}Cu_{30}$, and $Co_{30}Cu_{70}$, respectively. HRS—high resistance state, LRS—low resistance state.

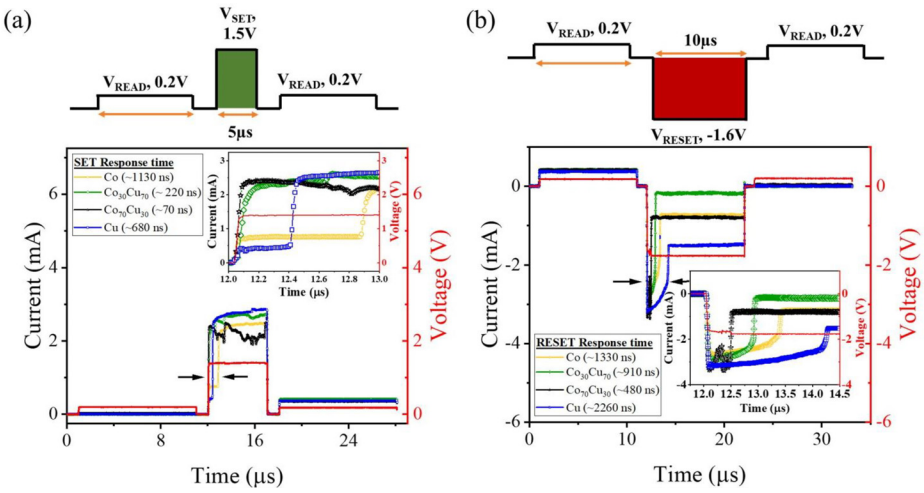

FIG. 3. (a) SET and (b) RESET response time characteristics of Pt/Ta_2O_5/Co (orange), Pt/Ta_2O_5/Cu (blue), Pt/Ta_2O_5/$Co_{70}Cu_{30}$ (black), and Pt/Ta_2O_5/$Co_{30}Cu_{70}$ (green) device. For SET and RESET responses, a 1.5 V/5 μs pulse and a −1.6 V/10 μs pulse are used, respectively. The red lines represent the input voltages. Inset provides the enlarged region of the current response for different active electrodes.

formed across the device is essential in the resistive switching performance for a CBRAM device.

Figure 3 shows the typical SET/RESET response time measurements of the CBRAM devices. READ pulses (0.2 V/10 μs) are applied before and after each SET/RESET operation to indicate the resistance states. The response time is obtained from the delay between the response current and the input voltage. The schematic diagrams at the top of Figs. 3(a) and 3(b) illustrate the voltage pulses used for SET and RESET operations, respectively, while the lower portion of Figs. 3(a) and 3(b) reveals the current change of the Co–Cu alloy CBRAM. A comparison of the SET/RESET response time for different devices is listed in Table I. Under a SET voltage pulse of 1.5 V/5 μs, the SET response time is ∼280 ns; under a RESET voltage pulse of −1.6 V/10 μs, the RESET response time is ∼620 ns. An improvement has also been observed for the $Co_{70}Cu_{30}$ alloy-based device, with the SET/RESET response times significantly reduced by up to 75%/51% (∼70 ns/∼480 ns), which is much faster than the Cu-based device (Table I). While for the pure Co electrode-based device, much longer response time is observed. The faster SET/RESET response time renders the $Co_{70}Cu_{30}$ alloy-based CBRAM devices to be more competitive in terms of data processing and storage application.

To gain more insight into the filaments formed in the Co–Cu alloy-based CBRAM devices, the temperature dependent resistance measurement is carried out for Co, Cu, and Co–Cu alloy CBRAM devices (Fig. S6). With each device at LRS, the R-T plot can be fitted by

TABLE I. Comparison of SET/RESET response time of Co, Cu, and Co–Cu alloy CBRAM.

Active electrode (AE)	Electrolyte	Inert electrode	SET response time (ns)	RESET response time (ns)
Co	Ta_2O_5	Pt	130	920
Cu	Ta_2O_5	Pt	280	620
$Co_{30}Cu_{70}$	Ta_2O_5	Pt	220	410
$Co_{70}Cu_{30}$	Ta_2O_5	Pt	70	480

$$R(T) = R_0[1 + \alpha(T - T_0)], \quad (1)$$

where R_0 is the reference resistance at temperature of T_0 and α is the temperature coefficient of resistance. The fitting results show a positive coefficient of 7.37×10^{-4} and 7.17×10^{-4} K^{-1} for Co and $Co_{70}Cu_{30}$ alloy CBRAM, respectively. This is consistent with the report by Yang *et al.*,[39] where a coefficient of 8.6×10^{-4} K^{-1} is obtained for the Co nanofilament. As for the Cu and $Co_{30}Cu_{70}$ alloy CBRAM, the fitting results indicate a positive coefficient of 3.09×10^{-3} and 1.01×10^{-3} K^{-1}, respectively. Both coefficient values agree with the values reported in literatures where the temperature coefficient of Cu nanofilament ranges from 1.45×10^{-3} to 4.5×10^{-3} K^{-1} (Refs. 40 and 41). In a Co–Cu alloy system, the standard electrode potential for Co^{2+}/Co is −0.28 V, which is substantially smaller than that of Cu^{2+}/Cu (0.34 V) and Co dissolve preferentially before Cu in the Co–Cu alloy.[42] The galvanic effect occurs between Co and Cu clusters where Co atoms will be oxidized into Co^{2+} ions by Cu ions.[43,44] Under the influence of an external electric field, the Co^{2+} ions migrate across the electrolyte, and Co filaments are formed.

In addition to the galvanic effect, the interface roughness between AE and the electrolyte also affects the filament formation process.[45,46] Near the ridges of the metal/electrolyte interface, the electrical field is much stronger than the surrounding regions, resulting in an increased propensity for filament formation. The surface and interfacial roughness of the different AEs were investigated using atomic force microscopy (AFM) and x-ray reflectivity (XRR). Figure 4 shows the interfacial roughness of the Co, Cu, $Co_{70}Cu_{30}$, and $Co_{30}Cu_{70}$ films with Ta_2O_5 film, and the AFM measurements are shown in Fig. S7. The surface and interfacial roughness results are summarized in Table II. Among all the films scanned, Cu has the highest roughness, from which an abrupt interface may be formed between Cu and Ta_2O_5. For Co and Co–Cu alloys, a typically smaller roughness is observed, with $Co_{70}Cu_{30}$ the smoothest. The $Co_{70}Cu_{30}$ film has the smallest average (R_a), root mean square (R_q), and interfacial (σ) values, that is, 0.30, 0.38, and 0.216 nm, respectively, which are much smaller than that of Co ($R_a = 0.39$ nm; $R_q = 0.49$ nm; $\sigma = 0.373$ nm). Nevertheless, even with a reduced roughness, the $Co_{70}Cu_{30}$ alloy-based device shows a smaller $V_{Forming}$ compared to the Co-based device [Figs. 1(d) and 1(e)].

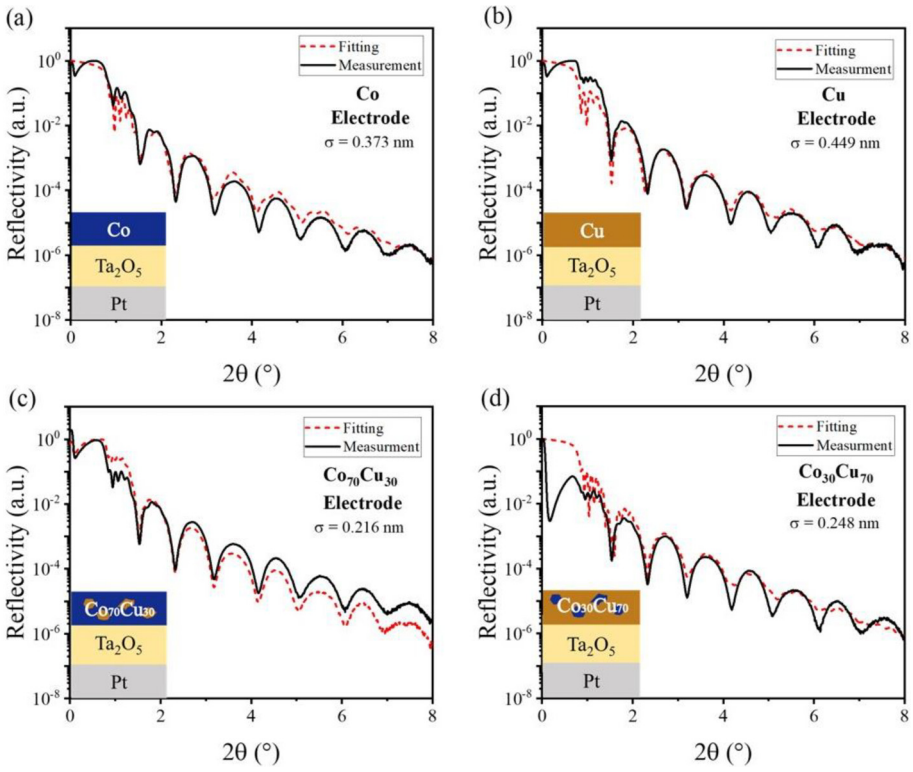

FIG. 4. XRR measurement and fitting of (a) Pt/Ta_2O_5/Co, (b) Pt/Ta_2O_5/Cu, (c) Pt/Ta_2O_5/$Co_{70}Cu_{30}$, and (d) Pt/Ta_2O_5/$Co_{30}Cu_{70}$ for interfacial roughness between Ta_2O_5 and TE.

In other words, the galvanic effect leads to the observed decrease in $V_{Forming}$ between $Co_{70}Cu_{30}$ and Co-based devices.

While a lower $V_{Forming}$ is observed for the $Co_{30}Cu_{70}$ alloy-based device, a more stable and uniform switching is obtained for the $Co_{70}Cu_{30}$ alloy-based device. This difference can be explained by considering the corrosion potential that varies logarithmically with the atomic percentage of Cu. The corrosion potential can be expressed as

$$E_{corr} = k - b_c \log[S_\theta], \tag{2}$$

where S_θ is the volume proportion and k and b_c are Tafel constants.[47] In a Co–Cu alloy system, due to the electrode potential difference between Co and Cu, as the Cu concentration increases, the corrosion rate of Co–Cu alloy increases. The acceleration of corrosion rate may lead to more nucleation sites; consequently, more filaments are formed. It has been reported that the randomness of filament formation typically has a poorer stability of switching performance.[38,48] By comparing with a higher Cu concentration of the $Co_{30}Cu_{70}$ alloy CBRAM, fewer yet more robust Co filaments tend to be formed for the $Co_{70}Cu_{30}$ alloy CBRAM as there are sufficient Co nucleation sites for Co filament formation. Based on this, a physical model illustrating the mechanism of Cu and Co filament formation is shown in Fig. 5. The higher corrosion reaction rate, coupled with increased roughness (see Table II), leads to the formation of a greater number of but less robust Cu filaments [Fig. 5(a), $Co_{30}Cu_{70}$], in contrast to that shown in Fig. 5(b) for the $Co_{70}Cu_{30}$ alloy-based device where Co filaments formation are present. The relative concentration between Co and Cu determines the corrosion rate and filament composition, which ultimately acts as an important role in the resistive switching characteristics. According to the proposed model, it is expected that optimizing the relative concentration of Cu in the Co–Cu alloy holds the potential to enhance the performance of the device.

TABLE II. Comparison of average, root mean square surface roughness, and interfacial roughness.

Active electrode (AE)	Average surface roughness, R_a (nm)	Root mean square surface roughness, R_q (nm)	Interfacial roughness, σ (nm)
Co	0.39	0.49	0.373
Cu	0.44	0.56	0.449
$Co_{30}Cu_{70}$	0.40	0.50	0.248
$Co_{70}Cu_{30}$	0.30	0.38	0.216

In conclusion, the resistive switching characteristics of Co–Cu alloy electrode CBRAM devices have been investigated. By utilizing $Co_{70}Cu_{30}$ alloy as the active electrode, reduced $V_{Forming}$ (~2 V), smaller V_{SET}/V_{RESET} distribution, narrower resistance states (HRS and LRS) variation, and shorter SET/RESET response time (~70 ns/~480 ns) have been realized. These enhanced switching performances are attributed to the formation of Co conductive filaments through a galvanic effect, where the electrochemical oxidation of Co atoms takes precedence over Cu atoms due to their respective electrode potentials. Additionally, a comparative analysis involving $Co_{30}Cu_{70}$ alloy underscores the significance of appropriate alloy composition in

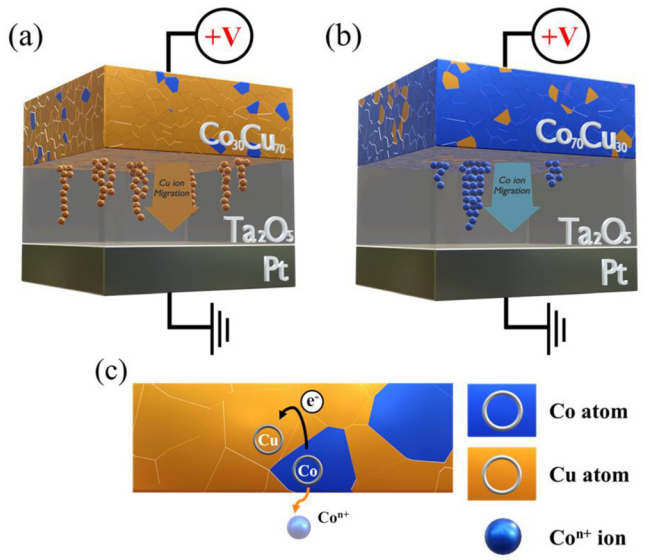

FIG. 5. Schematic diagrams of filament formation in different Co–Cu alloy-based CBRAM devices. (a) SET process of $Co_{30}Cu_{70}$ alloy CBRAM where the elemental composition of CFs are mainly Cu atoms due to the lack of Co atoms at the metal/electrolyte interface. (b) SET process of $Co_{70}Cu_{30}$ alloy CBRAM where the elemental composition of the CFs is mainly Co atoms. (c) Exchange of electrons between Cu and Co due to the galvanic effect.

determining CBRAM performance. The proposed approach and underlying mechanism not only develop a CBRAM with enhanced performance but also suggest that optimizing the alloy composition based on corrosion potential can achieve more uniform switching and larger memory window characteristics. This technique hold promises as a strategy for developing high-performance memory devices for application in high-speed and lower-power electronics.

See the supplementary material for the results of XPS analysis of Co–Cu alloy films, the boxplot distribution of V_{SET} and V_{RESET} for size random devices with different Co–Cu alloy AEs, the HRS and LRS boxplot comparison for each device stack with different AEs, the I–V curves of Ag–Cu alloy-based devices, the boxplot distribution of V_{SET} and V_{RESET} for Ag–Cu alloy-based devices, the resistance–temperature plot of Co–Cu alloy-based devices, and the AFM analysis of Co–Cu alloy films.

This work was supported by a RIE2020 ASTAR AME IAF-ICP (Grant No. I1801E0030) and EDB-IPP: Economic Development Board–Industrial Postgraduate Program (Grant No. REQ0165097).

AUTHOR DECLARATIONS

Conflict of Interest

The authors have no conflicts to disclose.

Author Contributions

Calvin Xiu Xian Lee: Conceptualization (equal); Data curation (equal); Investigation (equal); Methodology (equal); Visualization (equal); Writing – original draft (equal). **Putu Andhita Dananjaya:** Conceptualization (equal); Investigation (supporting); Writing – original draft (equal); Writing – review & editing (equal). **Mun Yin Chee:** Data curation (equal); Investigation (supporting); Writing – review & editing (equal). **Han Yin Poh:** Data curation (equal); Writing – review & editing (equal). **Funan Tan:** Investigation (equal); Visualization (equal); Writing – review & editing (equal). **Jia Rui Thong:** Data curation (supporting); Investigation (supporting); Resources (supporting). **Lingli Liu:** Data curation (supporting); Investigation (supporting). **Gerard Joseph Lim:** Writing – review & editing (supporting). **Yuanmin Du:** Investigation (equal); Methodology (supporting); Writing – review & editing (equal). **Juan Boon Tan:** Funding acquisition (equal); Supervision (equal); Writing – review & editing (equal). **Wen Siang Lew:** Conceptualization (equal); Funding acquisition (equal); Project administration (equal); Resources (equal); Supervision (equal); Writing – review & editing (equal).

DATA AVAILABILITY

The data that support the findings of this study are available within the article and its supplementary material.

REFERENCES

[1]K. H. Kim, S. Gaba, D. Wheeler, J. M. Cruz-Albrecht, T. Hussain, N. Srinivasa, and W. Lu, Nano Lett. **12**, 389 (2012).
[2]G. Zhu, W. Chen, D. Wang, H. Xie, Z. Zhao, P. Gao, J. Schutt-Aine, and W. Y. Yin, IEEE Trans. Electron Devices **66**, 1747 (2019).
[3]A. Chen, Solid State Electron. **125**, 25 (2016).
[4]S. C. W. Chow, P. A. Dananjaya, J. M. Ang, D. J. J. Loy, J. R. Thong, S. W. Hoo, E. H. Toh, and W. S. Lew, Appl. Surf. Sci. **608**, 155233 (2023).
[5]J. J. Yang, D. B. Strukov, and D. R. Stewart, Nat. Nanotechnol. **8**, 13 (2013).
[6]Q. Xia, W. Robinett, M. W. Cumbie, N. Banerjee, T. J. Cardinali, J. J. Yang, W. Wu, X. Li, W. M. Tong, D. B. Strukov, G. S. Snider, G. Medeiros-Ribeiro, and R. S. Williams, Nano Lett. **9**, 3640 (2009).
[7]H. Yeon, P. Lin, C. Choi, S. H. Tan, Y. Park, D. Lee, J. Lee, F. Xu, B. Gao, H. Wu, H. Qian, Y. Nie, S. Kim, and J. Kim, Nat. Nanotechnol. **15**, 574 (2020).
[8]M. Y. Chee, P. A. Dananjaya, G. J. Lim, Y. Du, and W. S. Lew, ACS Appl. Mater. Interfaces **14**, 35959 (2022).
[9]J. M. Ang, P. A. Dananjaya, S. C. W. Chow, G. J. Lim, C. S. Seet, and W. S. Lew, Nanotechnology **34**, 185202 (2023).
[10]D. Jana, S. Roy, R. Panja, M. Dutta, S. Z. Rahaman, R. Mahapatra, and S. Maikap, Nanoscale Res. Lett. **10**, 188 (2015).
[11]Y. M. Sun, C. Song, J. Yin, L. L. Qiao, R. Wang, Z. Y. Wang, X. Z. Chen, S. Q. Yin, M. S. Saleem, H. Q. Wu, F. Zeng, and F. Pan, Appl. Phys. Lett. **114**, 193502 (2019).
[12]M. Saadi, P. Gonon, C. Vallée, F. Jomni, E. Jalaguier, and A. Bsiesy, J. Mater. Sci. **31**, 13487 (2020).
[13]H. Wang, Y. Du, Y. Li, B. Zhu, W. R. Leow, Y. Li, J. Pan, T. Wu, and X. Chen, Adv. Funct. Mater. **25**, 3825 (2015).
[14]D. Jana, S. Chakrabarti, S. Z. Rahaman, and S. Maikap, Nanoscale Res. Lett. **10**, 392 (2015).
[15]H. J. Kim, T. H. Park, K. J. Yoon, W. M. Seong, J. W. Jeon, Y. J. Kwon, Y. Kim, D. E. Kwon, G. S. Kim, T. J. Ha, S. G. Kim, J. H. Yoon, and C. S. Hwang, Adv. Funct. Mater. **29**, 1806278 (2019).
[16]W. Banerjee and H. Hwang, Adv. Electron. Mater. **6**, 2000488 (2020).
[17]P. A. Dananjaya, D. J. J. Loy, S. C. W. Chow, and W. S. Lew, ACS Appl. Electron. Mater. **1**, 2076 (2019).
[18]Q. Liu, J. Sun, H. Lv, S. Long, K. Yin, N. Wan, Y. Li, L. Sun, and M. Liu, Adv. Mater. **24**, 1844 (2012).
[19]J. Yu, X. Xu, T. Gong, Q. Luo, D. Dong, P. Yuan, L. Tai, J. Yin, X. Zhu, X. Wu, H. Lv, and M. Liu, Nanoscale Res. Lett. **14**, 111 (2019).
[20]A. Saleem, F. M. Simanjuntak, S. Chandrasekaran, S. Rajasekaran, T. Y. Tseng, and T. Prodromakis, Appl. Phys. Lett. **118**, 112103 (2021).
[21]G. Baek, S. Yang, and T. Kim, Microelectron. Eng. **215**, 110987 (2019).

[22]H. Abbas, J. Li, and D. Ang, Micromachines **13**, 725 (2022).
[23]W. Banerjee, Electronics **9**, 1029 (2020).
[24]J. Woo and H. Hwang, ECS J. Solid State Sci. Technol. **5**, Q98 (2016).
[25]A. Belmonte, T. Witters, A. Covello, G. Vereecke, A. Franquet, V. Spampinato, S. Kundu, M. Mao, H. Hody, G. S. Kar, J. Radhakrishnan, L. Goux, G. L. Donadio, P. Kumbhare, A. Redolfi, R. Delhougne, L. Nyns, and W. Devulder, in *2019 IEEE International Electron Devices Meeting (IEDM)* (IEEE, 2019), pp. 35.8.1–35.8.4.
[26]J. Radhakrishnan, A. Belmonte, L. Nyns, W. Devulder, G. Vereecke, G. L. Donadio, P. Kumbhare, R. Delhougne, M. Houssa, G. S. Kar, and L. Goux, Appl. Phys. Lett. **117**, 151902 (2020).
[27]Y.-J. Choi, S. Bang, T.-H. Kim, K. Hong, S. Kim, S. Kim, B.-G. Park, and W. Y. Choi, ACS Appl. Electron. Mater. **5**, 1834 (2023).
[28]S. Yu and P. Y. Chen, IEEE Solid-State Circuits Mag. **8**, 43 (2016).
[29]F. Pan, S. Gao, C. Chen, C. Song, and F. Zeng, Mater. Sci. Eng. R **83**, 1 (2014).
[30]D. S. Jeong, R. Thomas, R. S. Katiyar, J. F. Scott, H. Kohlstedt, A. Petraru, and C. S. Hwang, Rep. Prog. Phys. **75**, 076502 (2012).
[31]L. Chen, Y. Xu, Q. Q. Sun, H. Liu, J. J. Gu, S. J. Ding, and D. W. Zhang, IEEE Electron Device Lett. **31**, 356 (2010).
[32]S. K. Vishwanath, H. Woo, and S. Jeon, Appl. Phys. Lett. **112**, 253503 (2018).
[33]H. Woo, S. K. Vishwanath, and S. Jeon, ACS Appl. Mater. Interfaces **10**, 8124 (2018).
[34]L. Goux, K. Sankaran, G. Kar, N. Jossart, K. Opsomer, R. Degraeve, G. Pourtois, G.-M. Rignanese, C. Detavernier, S. Clima, Y.-Y. Chen, A. Fantini, B. Govoreanu, D. J. Wouters, M. Jurczak, L. Altimime, and J. A. Kittl, in *2012 Symposium on VLSI Technology* (IEEE, 2012), pp. 69–70.
[35]W. Devulder, K. Opsomer, F. Seidel, A. Belmonte, R. Muller, B. De Schutter, H. Bender, W. Vandervorst, S. Van Elshocht, M. Jurczak, L. Goux, and C. Detavernier, ACS Appl. Mater. Interfaces **5**, 6984 (2013).
[36]L. Qiao, Y. Sun, C. Song, S. Yin, Q. Wan, J. Liu, R. Wang, F. Zeng, and F. Pan, J. Phys. Chem. C **124**, 11438 (2020).
[37]Y. T. Tseng, I. C. Chen, T. C. Chang, J. C. Huang, C. C. Shih, H. X. Zheng, W. C. Chen, M. H. Wang, W. C. Huang, M. C. Chen, X. H. Ma, Y. Hao, and S. M. Sze, Appl. Phys. Lett. **113**, 053501 (2018).
[38]J. Wang, G. Cao, K. Sun, J. Lan, Y. Pei, J. Chen, and X. Yan, Nanoscale **14**, 1318 (2022).
[39]Z. Yang, Q. Zhan, X. Zhu, Y. Liu, H. Yang, B. Hu, J. Shang, L. Pan, B. Chen, and R. W. Li, EPL **108**, 58004 (2014).
[40]G. Schindler, G. Steinlesberger, M. Engelhardt, and W. Steinhögl, Solid State Electron. **47**, 1233 (2003).
[41]Q. Huang, C. M. Lilley, M. Bode, and R. S. Divan, in *2008 8th IEEE Conference on Nanotechnology* (IEEE-NANO, 2008), p. 549.
[42]S. Yang, B. Zhang, Q. Zhang, R. Wang, X. Yu, C. Wang, and Y. Liu, ECS J. Solid State Sci. Technol. **8**, P416 (2019).
[43]R. Nafria, A. Genç, M. Ibáñez, J. Arbiol, P. Ramírez De La Piscina, N. Homs, and A. Cabot, Langmuir **32**, 2267 (2016).
[44]X. Xia, Y. Wang, A. Ruditskiy, and Y. Xia, Adv. Mater. **25**, 6313 (2013).
[45]M. Al-Mamun, S. W. King, and M. Orlowski, ECS J. Solid State Sci. Technol. **8**, N220 (2019).
[46]T. A. De Assis, F. Borondo, R. M. Benito, and R. F. S. Andrade, Phys. Rev. B **78**, 235427 (2008).
[47]J. Idrac, G. Mankowski, G. Thompson, P. Skeldon, Y. Kihn, and C. Blanc, Electrochim. Acta **52**, 7626 (2007).
[48]J. Park, H. Jeon, H. Kim, W. Jang, H. Seo, and H. Jeon, RSC Adv. **4**, 61064 (2014).